AFRL-HE-WP-TR-2003-0019

UNITED STATES AIR FORCE RESEARCH LABORATORY

DEVELOPMENT OF HIGH PERFORMANCE PNEUMATIC MUSCLE ACTUATOR SYSTEMS

Rupa Purasinghe

CALIFORNIA STATE UNIVERSITY
LOS ANGELES CA 90032

Maria Feng

FENG ENTERPRISES
NEWPORT BEACH CA 92657

Masanobu Shinozuka

UNIVERSITY OF SOUTHERN CALIFORNIA
LOS ANGELES CA 90089

NOVEMBER 1999

FINAL REPORT FOR THE PERIOD 15 MAY 1998 TO 30 NOVEMBER 1999

Human Effectiveness Directorate
Crew System Interface Division
2255 H Street
Wright-Patterson AFB OH 45433-7022

NOTICES

When US Government drawings, specifications, or other data are used for any purpose other than a definitely related Government procurement operation, the Government thereby incurs no responsibility nor any obligation whatsoever, and the fact that the Government may have formulated, furnished, or in any way supplied the said drawings, specifications, or other data, is not to be regarded by implication or otherwise, as in any manner licensing the holder or any other person or corporation, or conveying any rights or permission to manufacture, use, or sell any patented invention that may in any way be related thereto.

Please do not request copies of this report from the Air Force Research Laboratory. Additional copies may be purchased from:

National Technical Information Service
5285 Port Royal Road
Springfield, Virginia 22161

Federal Government agencies and their contractors registered with the Defense Technical Information Center should direct requests for copies of this report to:

Defense Technical Information Center
8725 John J. Kingman Road, Suite 0944
Ft. Belvoir, Virginia 22060-6218

DISCLAIMER

This Technical Report is published as received and has not been edited by the Air Force Research Laboratory, Human Effectiveness Directorate.

TECHNICAL REVIEW AND APPROVAL

AFRL-HE-WP-TR-2003-0019

This report has been reviewed by the Office of Public Affairs (PA) and is releasable to the National Technical Information Service (NTIS). At NTIS, it will be available to the general public.

This technical report has been reviewed and is approved for publication.

FOR THE COMMANDER

MARIS M. VIKMANIS
Chief, Crew System Interface Division
Air Force Research Laboratory

REPORT DOCUMENTATION PAGE

Form Approved
OMB No. 0704-0188

1. AGENCY USE ONLY (Leave blank)	2. REPORT DATE	3. REPORT TYPE AND DATES COVERED
	November 1999	Final, 15 May 1998 - 30 November 1999

4. TITLE AND SUBTITLE

Development of High Performance Pneumatic Muscle Actuator Systems

5. FUNDING NUMBERS

C: F41624-98-1-001
PR: 7184
TA: 08
WU: LA

6. AUTHOR(S)

*Rupa Purasinghe, **Maria Feng, ***Masanobu Shinozuka

7. PERFORMING ORGANIZATION NAME(S) AND ADDRESS(ES)

* California State University, Los Angeles CA 90032
** Feng Enterprises, Newport Beach CA 92657
***University of Southern California, Los Angeles CA 90089

8. PERFORMING ORGANIZATION

9. SPONSORING/MONITORING AGENCY NAME(S) AND ADDRESS(ES)

Air Force Research Laboratory
Human Effectiveness Directorate
Crew System Interface Division
Air Force Materiel Command
Wright-Patterson AFB OH 45433-7022

10. SPONSORING/MONITORING

AFRL-HE-WP-TR-2003-0019

11. SUPPLEMENTARY NOTES

12a. DISTRIBUTION/AVAILABILITY STATEMENT

Approved for public release; distribution is unlimited

12b. DISTRIBUTION CODE

13. ABSTRACT *(Maximum 200 words)*

In this project, a prototype pneumatic muscle actuator system resembling a human arm joint has been designed, fabricated, and tested. System identification of the actuator system with different types, sizes, and characteristics of rubber muscles were performed through static and dynamic tests, and experimental as well as theoretical models were developed. Control algorithms including a feed-forward algorithm suitable for the muscle actuator system was developed and implemented to compensate the time delay otherwise inherent in the response of the actuator system. The time delay of the muscle response depended on the type and size of the muscles. The larger muscle suffered larger time delay, although it provided larger power and stroke. The control algorithm equipped with the feed-forward compensation developed in this research is very effective in reducing the time delay in response. Excellent control performance of the pneumatic muscle actuator system was confirmed by experiments. This research has demonstrated the potential of using pneumatic muscle actuators for enhancing human strength and mobility.

14. SUBJECT TERMS	15. NUMBER OF PAGES
Pneumatic muscle actuator systems	49
	16. PRICE CODE

17. SECURITY CLASSIFICATION OF REPORT	18. SECURITY CLASSIFICATION OF THIS PAGE	19. SECURITY CLASSIFICATION OF ABSTRACT	20. LIMITATION OF ABSTRACT
Unclassified	Unclassified	Unclassified	Unlimited

NSN 7540-01-280-5500

Standard Form 298 (Rev 2-89) Prescribed by ANSI Std Z-39-18
298-102 COMPUTER GENERATED

THIS PAGE IS INTENTIONALLY LEFT BLANK

Table of Contents

List of Illustrations

List of Tables

Acknowledgement of Sponsorship

This research effort was sponsored by the AFRL/HECP, Air Force Material Command, USAF, under grant number F41624-98-1-0001, with Dr. Daniel Repperger as the Program Manager.

THIS PAGE INTENTIONALLY LEFT BLANK

1. Introduction

1.1. Background

Pneumatic artificial muscle actuators were first developed in artificial limb research in the 1950's and 1960's (Gavrilovic and Maric, 1969, Schulte, 1961). They were commercialized by the Bridgestone Corporation, Japan, in the 1980's (Inoue, 1988) using rubber as the primary muscle material for robotics applications (e.g., Feng, et al, 1997, Hesselroth, et al, 1994, Uno, 1986, Yamafuji, et al, 1993). These actuators have high power-to-weight and power-to-volume ratios and flexible mechanical features friendly to human as compared to hydraulic and electric actuators. Therefore, these actuators have shown considerable potential for enhancing human strength and mobility for military as well as civilian applications.

However, some features of the pneumatic actuators, namely the compressibility of the air inside the muscles, the delay of the response and its nonlinearity for example, make it difficult to precisely control output displacements and forces of these actuators, which prevents their effective applications in the fields as mentioned above.

Significant efforts have recently been made to overcome such drawbacks. For example, Repperger, et al, (1997) performed static and dynamic tests on a pneumatic muscle actuator system to identify its nonlinear characteristics and to incorporate them into a force control algorithm. Chou et al (1996) developed a linearized model of the McKibben artificial muscle pneumatic actuator. Galdwell et al (1995) applied the adaptive control scheme combined on on-line system identification to improve the accuracy of the position control. Hesselroth, et al (1994) developed a neural learning

algorithm for position control of a robot arm actuated by rubber muscles. The previous, work represented by these papers contributed significantly to the artificial muscle technology. Additional work, however, is needed to further improve the control performance of pneumatic muscles in order to make them implementable.

1.2. Objective of this Research

The objectives of this research are

i) to develop a prototype pneumatic muscle actuator system reflecting the state of the art technology.

ii) to study and model its static and dynamic characteristics and

iii) to develop and apply effective control algorithms to achieve accurate position control.

2. Development of a Pneumatic Muscle Actuator System

2.1. Characteristics of Pneumatic Air Muscles

The pneumatic muscles used as actuators in this research are called *McKibben Pneumatic Artificial Air Muscles*. The muscle has an internal rubber bladder covered with an external shell formed from interwoven nylon fibers (Figure 2.1). When the internal bladder is pressurized, the high pressure air pushes against its inner surface and its external shell, and thus tends to increase its volume. The bladder and thread are fixed at both ends tightly with fittings. Due to the non extensibility (or very high longitudinal stiffness) of the nylon fibers of the external shell, the muscle shortens according to its volume increase and/or tension force if it is coupled to a mechanical load. By combining a pair of such muscles in different ways and by controlling the pressure difference of the air inside the two muscle bladders, one can provide various actuations.

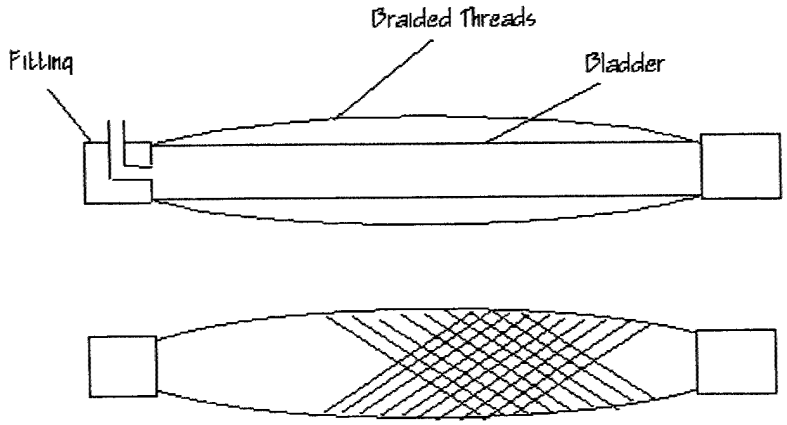

Figure 2.1: Structure of McKibben Pneumatic Artificial Muscle

Three types of pneumatic muscles were used for the experiment. The specifications of each muscle are shown in Table. 2.1.

Table 2.1: Specifications of each Muscle

Model	*AM-02*
Manufacturer	**Shadow Robot Co.**
Length	**210 [mm]**
Diameter	**20 [mm]**
Load pulled at 50 psi	**45 [lb.]**
Percent contraction per given load	**25% Contraction with load of: 25 [lb.]**

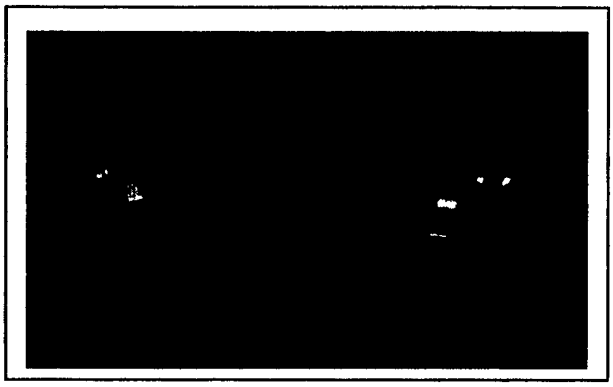

Model	*AM-04*
Manufacturer	**Shadow Robot Co.**
Length	**400 [mm]**
Diameter	**50 [mm]**
Load pulled at 50 psi	**300 [lb.]**
Percent contraction per given load	**25% Contraction with load of: 150 [lb.]**

Model	*RUB-125*
Manufacturer	**Bridgestone**
Length	**280 [mm]**
Diameter	**15 [mm]**
Load pulled at 50 psi	**140 [lb.]**
Percent contraction per given load	**20% Contraction with load of: 30.8 [lb.]**

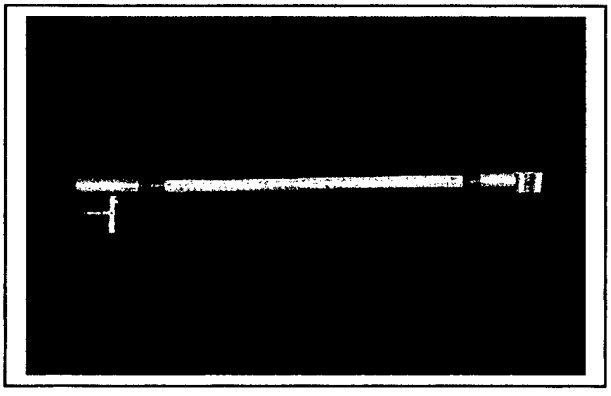

2.2. Experimental Setup of One-Linked Arm Fixture

An experimental setup of a one-linked arm fixture was designed and fabricated. As shown in Figure. 2.2, the system consists of a pair of muscles, an air compressor, two proportional pressure control valves, an air regulator, an encoder, two pressure sensors, a rotary link, and a computer with AD/DA boards. The muscles are connected through a pulley, which represents an arm joint. The angular position of the joint is controlled by adjusting the longitudinal deformation of each air muscle through controlling the air pressure inside the muscle. The encoder is used to measure the angular position of the joint and the two pressure sensors are used to monitor the air pressure inside each muscle. The measured data from these sensors are sent to the computer through the analog to digital (A/D) converter. The pressure control signals are sent to the air valve from the computer via the digital to analog (D/A) converter. Figure 2.3 is a photo of the fixture.

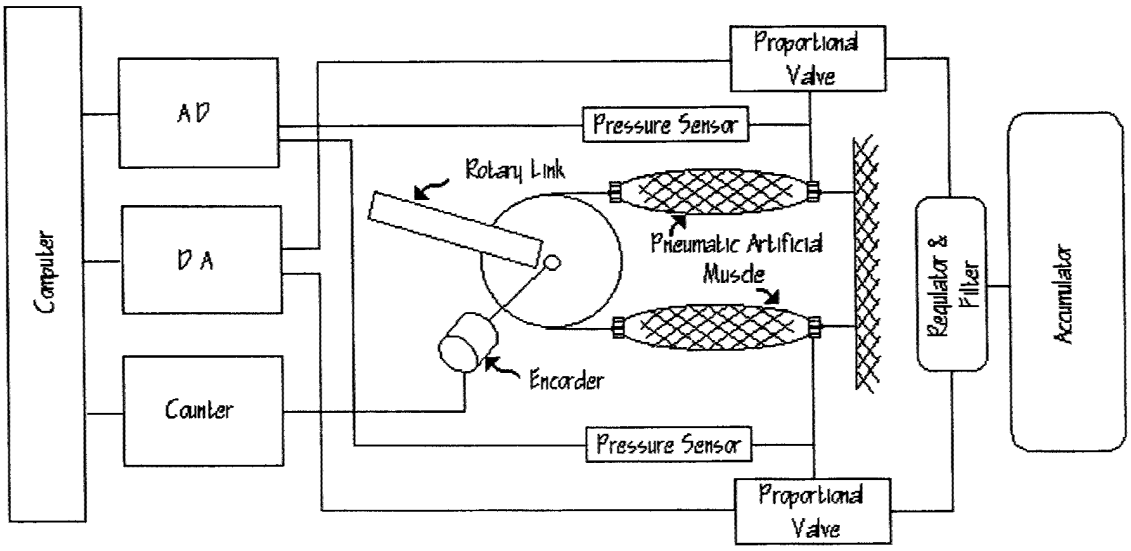

Figure 2.2: Schematic Diagram of Fixture

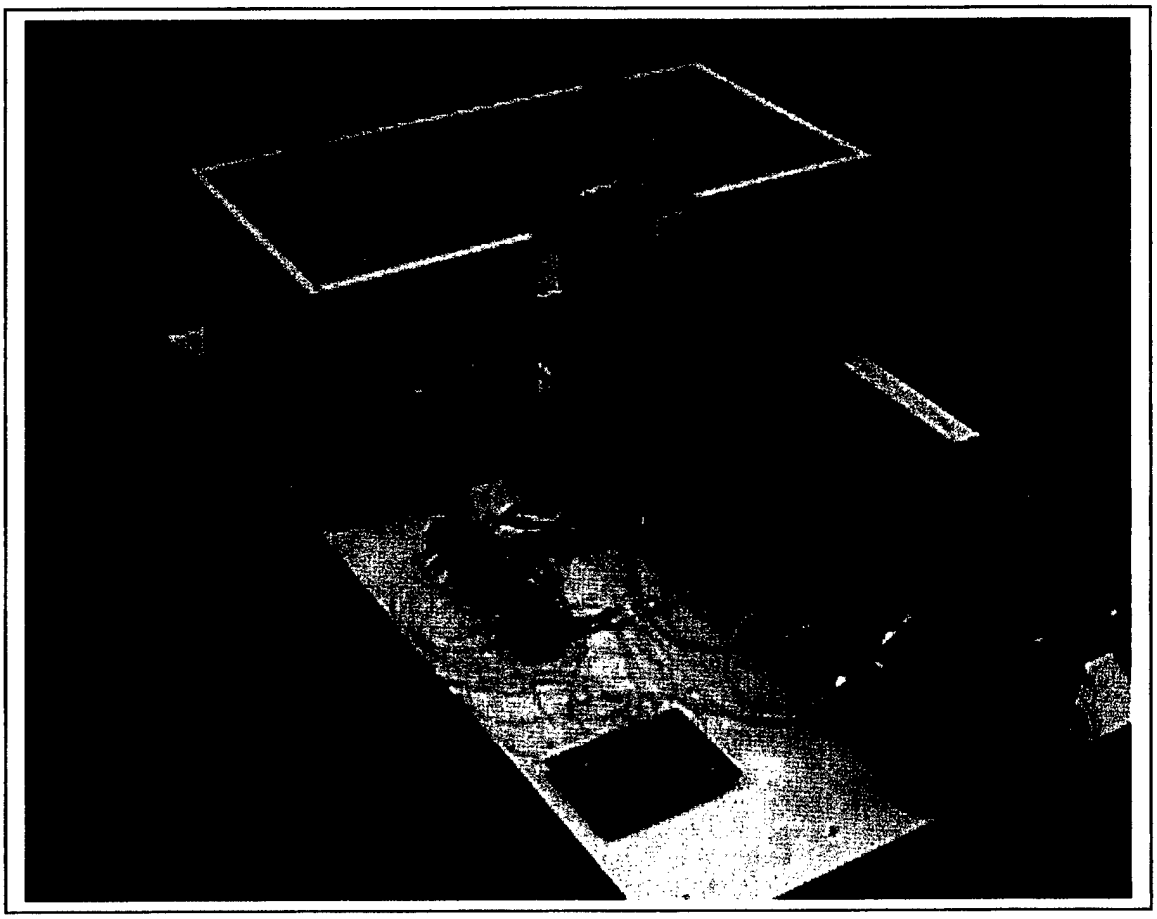

Figure 2.3: Photo of Fixture

2.3. Specifications of Devices used in the Experiment

The specifications of the valves, pressure sensors, encoder, A/D and D/A converters and the air compressor are shown in Table 2.2, through Table 2.6. Figures 2.4 through 2.8 show the photos of these devices.

Table 2.2: Specifications of Magnetic Proportional Pressure Control Valve

Model	***PPC5B-AAA-AGCA***
Manufacturer	**Fluidtrols Corporation**
Pressure Range	**100 (psi)**
Pressure Reference	**Gage Pressure**
Overall Accuracy	**□ 0.5% F.S.**
Command signal	**0-10 V Differential**

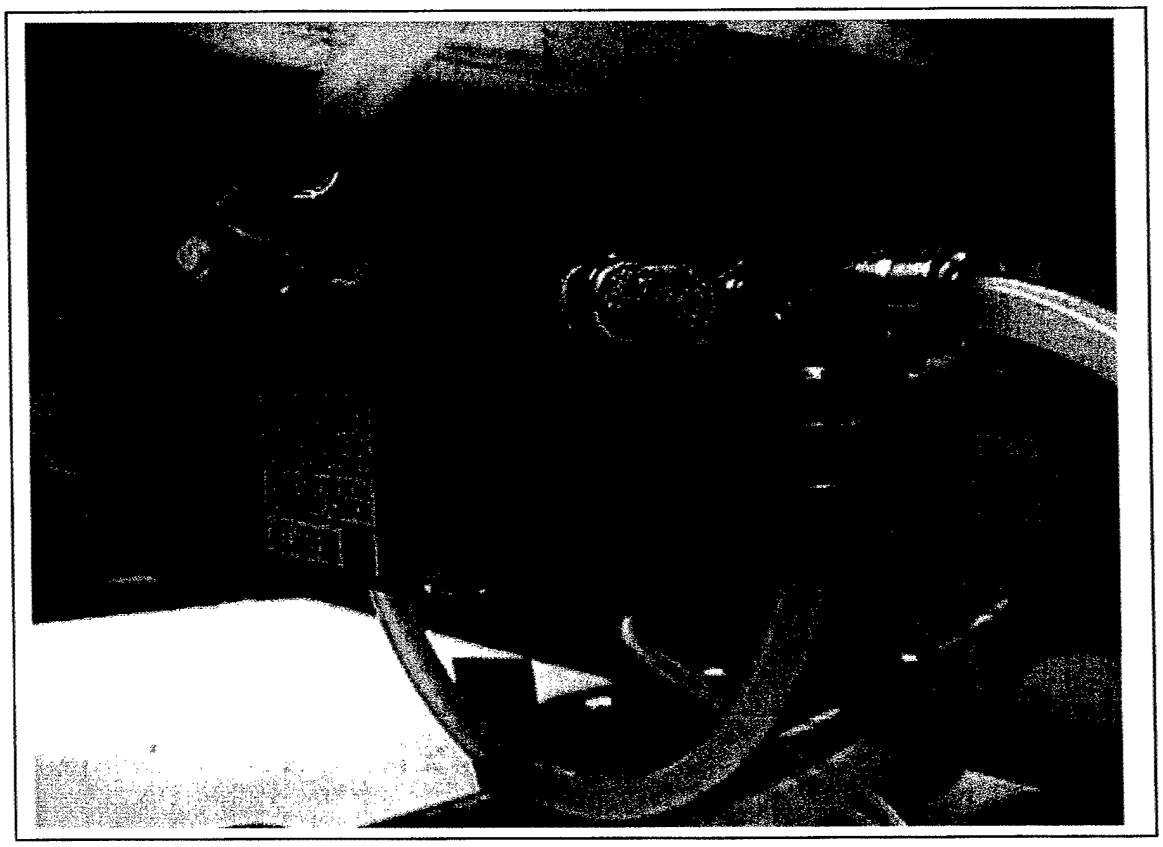

Figure 2.4: Pressure Valve

Table 2.3: Specifications of Pressure Sensor

Model	*DP2-42N*
Manufacturer	**SUNX**
Type of Pressure	**Gage Pressure**
Rotate Pressure Range	**0 ~ 1.000Mpa**
Applicable Fluid	**Non-corrosive gas**
Supply Voltage	**12 to 24 V DC $^{+10\%}_{-15\%}$** **Ripple P□P: 105 or less**
Output Voltage	**1 to 5 V** **Zero-point: within** **1V □ 5% F.S.** **Span: within 4V □ 5% F.S.** **Linearity: within V □ 5% F.S.**

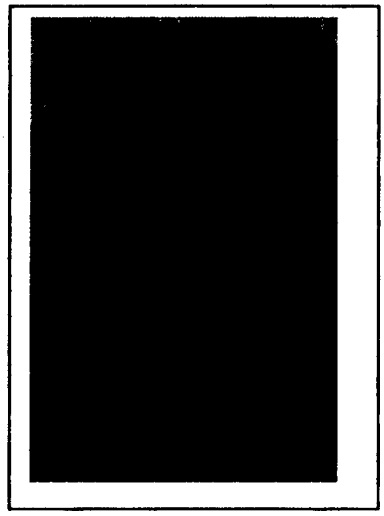

Figure 2.5: Pressure Sensor

Table 2.4: Specifications of Rotary Encoder

Model	*L25G-F1-2500-P4C-8830-LED-SM16*
Manufacturer	**BEI Sensors & Systems Company**
Code	**Incremental**
Count per Rotate	**10,000**
Maximum RPM	**10,000**
Moment of Inertia	**4.1 x 10^{-4} oz-in-sec^2**
Voltage Supply	**+5V de**
Output Format	**2 channels (cw & ccw)**
Frequency	**100 kHz**

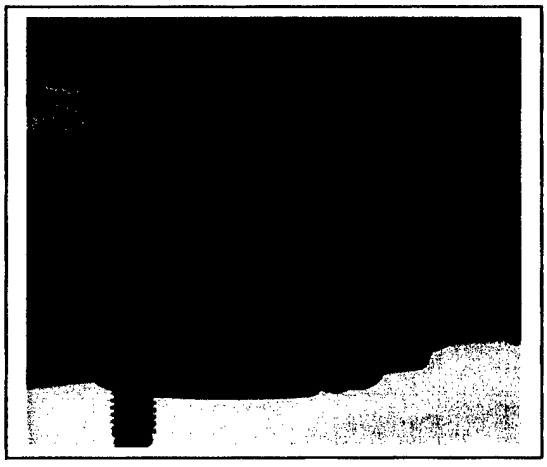

Figure 2.6: Rotary Encoder

Table 2.5: Specifications of Multifunction I/O Board

Model	*PCI-6024E*
Manufacturer	**National Instruments**
Analog Input	**16 Single-ended or 8 differential** **200kS/s sampling rate** **200kS/s stream-to-disk rate** **12 bit resolution**
Analog Output	**2channels** **12-bit resolution**
Digital I/O	**8 (5V/TTL) lines**
Counter / Timer	**2 up/down** **24 bit resolution**
Triggering	**Digital**

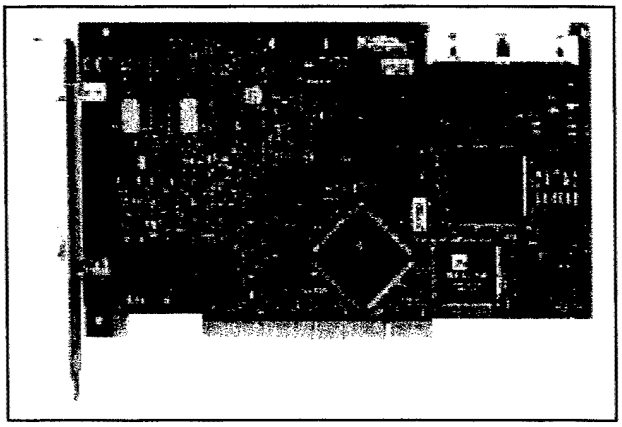

Figure 2.7: Multifunction I/O Board

Table 2.6 Specifications of Air Compressor

Model	*WL340003AJ*
Manufacturer	**CAMPBELL HAUSFELD**
Maximum Pressure	**125 psi**
Container Volume	**13 gallon**

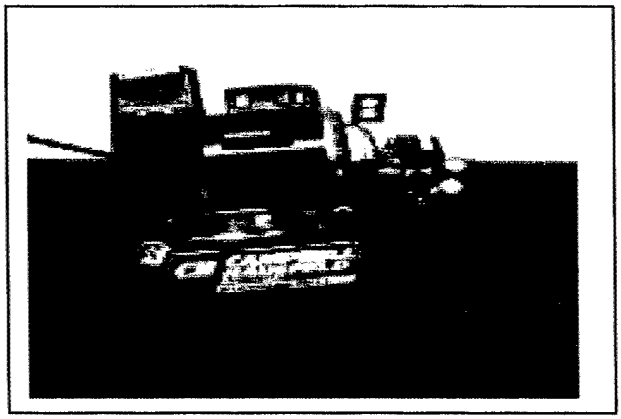

Figure 2.8: Air Compressor

3. Characteristics of Experimental Fixture

3.1. Theoretical Modeling of Air Muscle

In order to control the angular position or the torque of the arm joint through controlling the pressure of the air muscle, the relationship between the muscle force, air pressure and the contraction ratio of the muscle must be identified. In this research, a theoretical relationship was first derived. In order to simplify the model the following assumptions were made.

- The shape of the braided sleeve is cylindrical.
- The threads in the braided mesh shell are not extensible.
- The elasticity of bladder is ignored.
- The friction of each thread is ignored.

As depicted in Figure 3.1, the length of the muscle, L, has the following relationships with the contraction ratio ε, and the initial length L_n.

$$\begin{aligned} L &= (1-\varepsilon)L_n \\ L' &= (1-\varepsilon)L'_n \end{aligned} \tag{3.1}$$

where

L = Length of the muscle

L_n = Initial length of the muscle

L' = Longitudinal length of the muscle for one turn of thread.

L' = Initial longitudinal length of the muscle for one turn of thread.

As such

$$\begin{aligned} L_n &= mL'_n \\ L &= mL' \end{aligned} \tag{3.2}$$

where m = number of turns of thread

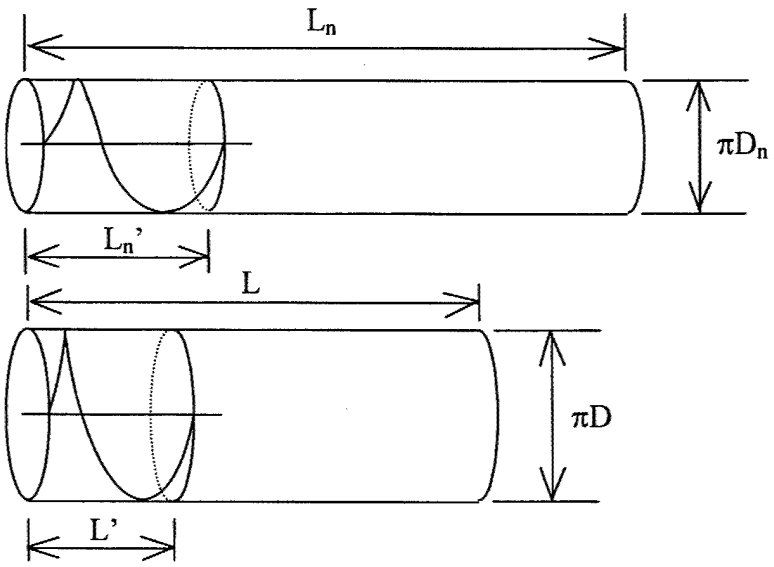

Figure 3.1: Simple Model of Air Muscle

The relationship between the above parameters are illustrated in the triangles shown in the Figure 3.2

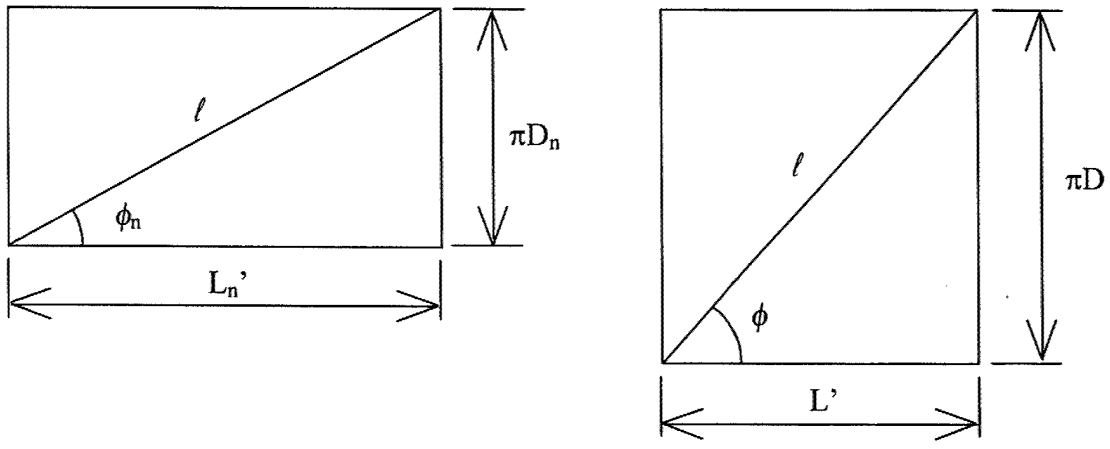

(a) Initial State (b) Contracted State

Figure 3.2: Geometry of Thread of Muscle

The geometry of the parameters of the triangle is as follows

$$(\pi D_n)^2 + L_n'^2 = (\pi D)^2 + L'^2 = l^2 \tag{3.3}$$

where D_n and D are at initial and final conditions of the air muscle, respectively.

By solving for D, yields

$$D^2 = D_n^{\,2} + \frac{L_n'^2}{\pi^2}\left\{1 - (1-\varepsilon)^2\right\} \tag{3.4}$$

Using the same geometry and solving for the circumference, yields

$$\begin{aligned} \pi D_n &= L_n' \tan\phi_n \\ \pi D &= L' \tan\phi \end{aligned} \tag{3.5}$$

where, ϕ_n and ϕ refer to the gradient angle of each thread at initial and contracted states.

Thus, setting the circumference equal to each other and solving, yields

$$\frac{D}{\tan\phi} = \frac{(1-\varepsilon)D_n}{\tan\phi_n} \tag{3.6}$$

Similarly,

$$L_n = ml\cos\phi_n \tag{3.7}$$

and

$$l = \frac{\pi D_n}{\sin\phi_n} \tag{3.8}$$

which yields,

$$L_n = \frac{\mathrm{m}\pi D_n}{\tan\phi_n} \tag{3.9}$$

By substituting Equation 3.9 into Equation 3.4, yields,

$$D^2 = D_n^{\,2}\left\{1 + \frac{(1-(1-\varepsilon)^2)}{\tan^2\phi_n}\right\} \tag{3.10}$$

and,

$$L\tan\phi = m\pi D \tag{3.11}$$

$$L = \frac{m\pi D}{\tan\phi} \tag{3.12}$$

The relationship between circular direction Force Fc and longitudinal Force F_L generated by the braided sleeve, can be expressed using angle ϕ as follows:

$$F_C : F_L = \sin\phi : \cos\phi \tag{3.13}$$

Thus,

$$F_C = \tan\phi \; F_L \tag{3.14}$$

Considering the free body diagram of the air muscle in Figure 3.3, yields

$$2\Delta f_C = P \cdot r \int_0^{\pi} \sin\phi \; d\phi = PD \tag{3.15}$$

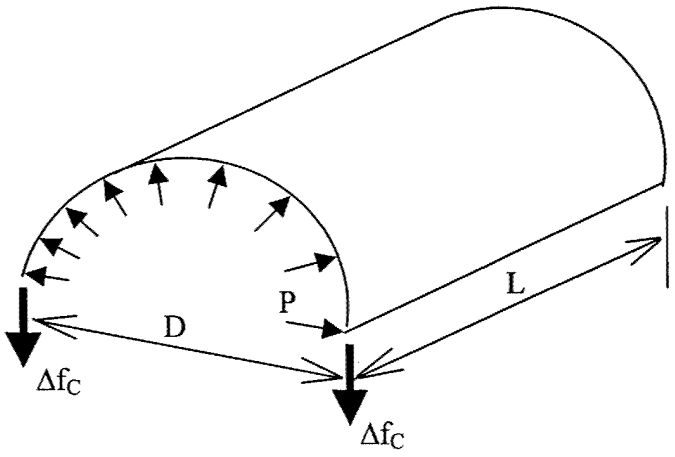

Figure 3.3: Circular Force

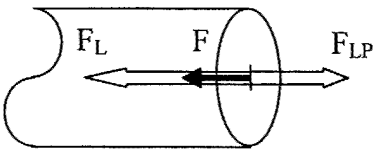

Figure 3.4: Balance of Longitudinal Forces

where,

Δf_C = the circular force that act on a small portion of the air muscle.

P = the pressure inside the air muscle.

r, D = the radius and the diameter of the muscle respectively.

Assuming F_C is the circular Force that is generated in the length of a one turn of thread, then

$$F_C = \Delta f_C L'$$

Thus,

$$2F_C = PDL' \tag{3.16}$$

Thus,

$$F_C = \frac{PDL'}{2} \tag{3.17}$$

The longitudinal force generated by internal air pressure F_{LP} is shown as:

$$F_{LP} = -EP \tag{3.18}$$

where, the force pointing towards the inside of the muscle is assumed the positive direction, and

E = cross section of the air muscle.

$$E = \frac{1}{4}\pi D^2 \tag{3.19}$$

Thus,

$$F_{LP} = -\frac{1}{4}\pi D^2 P \tag{3.20}$$

and, the contraction force of air muscle, F is the balancing force as shown in Figure 3.4.

$$F = F_L + F_{LP} \tag{3.21}$$

i.e.

$$F_L = F + \frac{1}{4}\pi D^2 P \tag{3.22}$$

Now substituting Equation 3.17 and Equation 3.22 into Equation 3.14, yields

$$F + \frac{1}{4}\pi D^2 P = \frac{PDL'}{2\tan\phi} \tag{3.23}$$

Substituting Equation 3.12 into Equation 3.23 yields the theoretical Equation,

$$F + \frac{1}{4}\pi D^2 P = \frac{\pi P}{2} \cdot \left(\frac{D}{\tan\phi}\right)^2 \tag{3.24}$$

By substituting Equation 3.24 into Equation 3.6, yields

$$F + \frac{1}{4}\pi D^2 P = \frac{\pi {D_n}^2 (1-\varepsilon)^2}{2\tan^2\phi_n} P \tag{3.25}$$

By substituting Equation 3.25 into Equation 3.10, yields

$$F = \frac{\pi {D_n}^2 P}{4\sin^2\phi_n}\left\{3\cos^2\phi_n (1-\varepsilon)^2 - 1\right\} \tag{3.26}$$

Thus, the theoretical model of the relationship of the muscle force, contraction ratio and the pressure can be expressed as

$$\boldsymbol{F} = A(\boldsymbol{B}(1-\varepsilon)^2 - 1)\boldsymbol{P} \tag{3.27}$$

where,

$$A = \frac{\pi {D_n}^2}{4\sin^2\phi_n}$$
$$B = 3\cos^2\phi_n \tag{3.28}$$

3.2. Experimental Modeling of Air Muscle

The theoretical model in Equation 3.27, which shows the relationship between the force, pressure and contraction ratio of each muscle is obtained in the Section 3.1. However, theoretical and experimental data do not agree perfectly with each other as shown in Figures. 3.5 a, b, and c. The two curves of the experimental results are for the forward and backward motions respectively. The force value for each contraction ratio from the experiments is generally lower than the value from the theoretical model. The difference may be due to such reasons as the assumption of uniform cross section of the muscle, the friction being ignored for each thread, and the elasticity of the bladder being ignored.

Therefore the experimental models are also obtained for each of the muscles, RUB-125, AM-02 and AM-04. Figures 3.6, 3.8, and 3.10 show the best-fitted straight lines of the experimental data for three different pressure values.

As shown in Figure 3.6, the experimental data approximates a straight line within the tested range of the pressure and contraction ratio (shown in Table 3.1) when hysteresis is ignored. Furthermore, the slope of the line is proportional to the pressure. The force value at $\varepsilon = 0$ is also in proportion to the pressure.

Table 3.1: Condition for Experiment

	RUB-125	AM-02	AM-04
Pressure Range[psi]	20 ~ 40	20 ~ 40	20 ~ 50
Range of Contraction Ratio ε	0.02 ~ 0.196	0.167 ~ 0.233	0.20 ~ 0.270
Total Stroke Range of ε	0.0 ~ 0.2	0.0 ~ 0.3	0.0 ~ 0.3

Therefore, the experimental model showing the relationship among the muscle force, contraction ratio and pressure can be expressed in the Equation shown below.

$$F = (aP + b)\varepsilon + (cP + d) \tag{3.29}$$

where P = pressure

a,b,c, and d are constants.

Table 3.1 lists the contraction and pressure ranges for each type of muscles for which the force-contraction ratio relationship can be linearized. Figures 3.7, 3.9 and 3.11 show the amount of error between the above mentioned experimental data and their best fit linear lines.

For the RUB-125 muscle, Figure 3.6 shows the linear relationships at three pressure states; 28.4, 42.6, 56.8[psi] (2, 3, 4 [kgf/cm^2]). The maximum stroke (contraction ratio) of the RUB-125 muscle is 0.2. The range of the contraction ratio tested in the experiment is 0.02 to 0.196, which covers 97 [%] of the entire range. Choosing the parameters, a, b, c and d in the Equation 3.29 to best fit the experimental data, the error between the approximated line and the experimental data of force values can be minimized below 15 [%], as shown in Figure. 3.7.

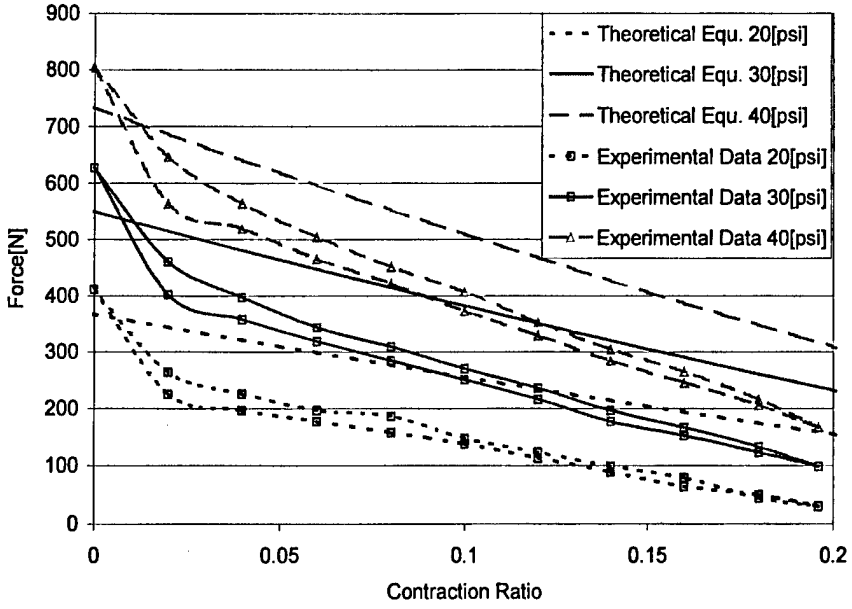

(a) RUB-125 Muscle

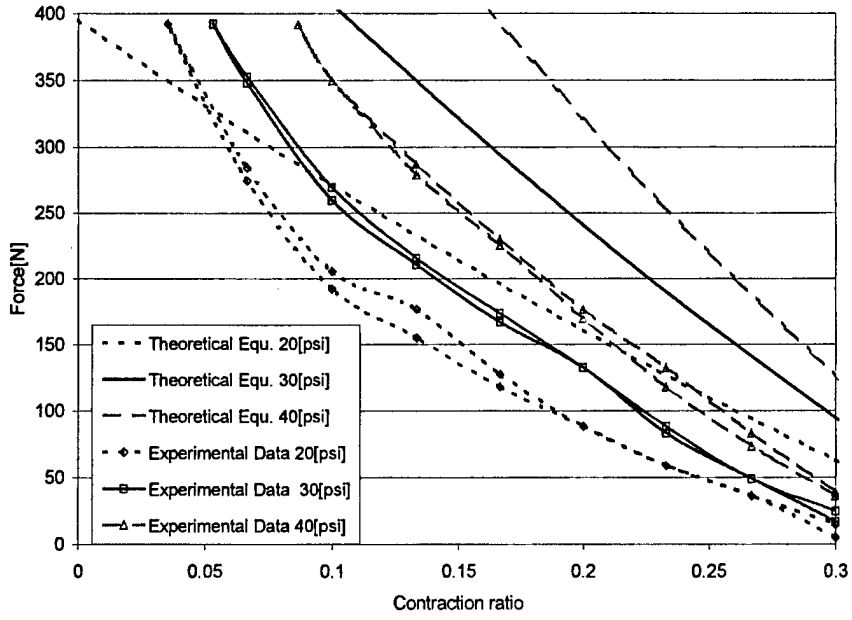

(b) AM-02 Muscle

Figure 3.5 (a) & (b): Relationship between Force and Contraction Ratio

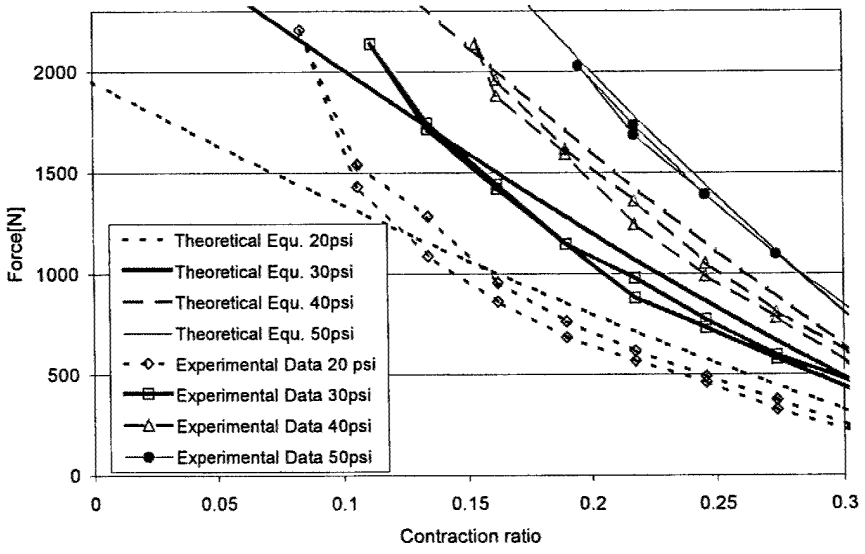

(c) AM-04 muscle

Figure 3.5(c): Relationship between Force and Contraction Ratio

Similarly, for muscles, AM-02 and AM-04, as shown in Figure 3.8 to Figure 3.11, the range of the contraction ratio which results in the error less than 15% are 22% and 23% respectively of the entire range of stroke.

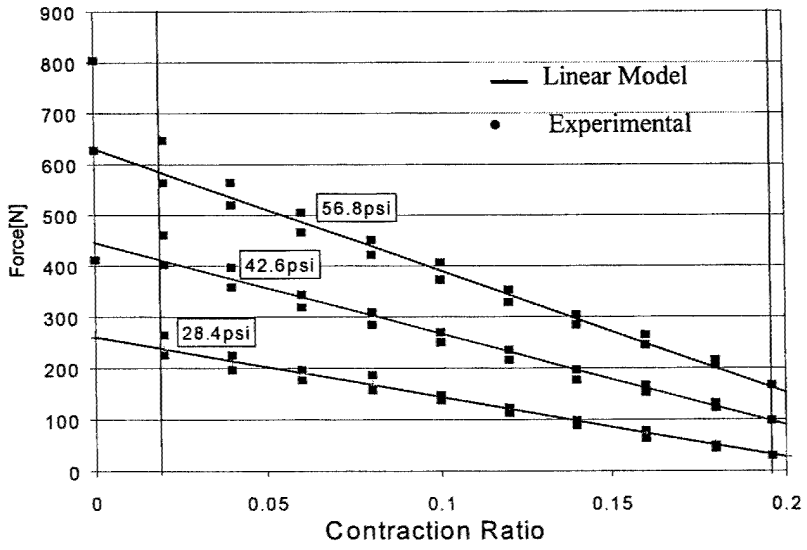

Figure 3.6: Experimental Modeling (RUB-125)

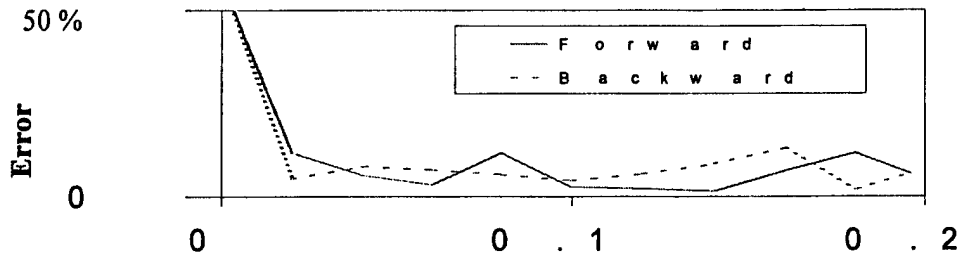

(a) P=28.4[psi]

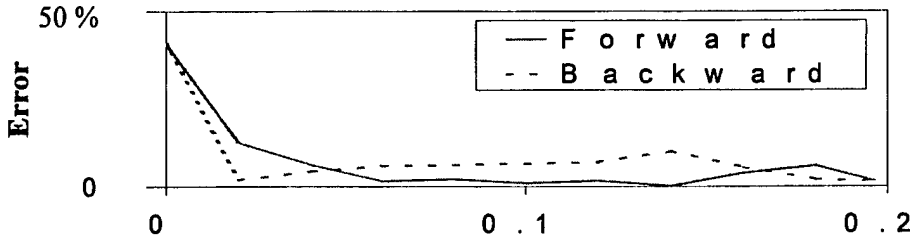

(a) P=42.6[psi]

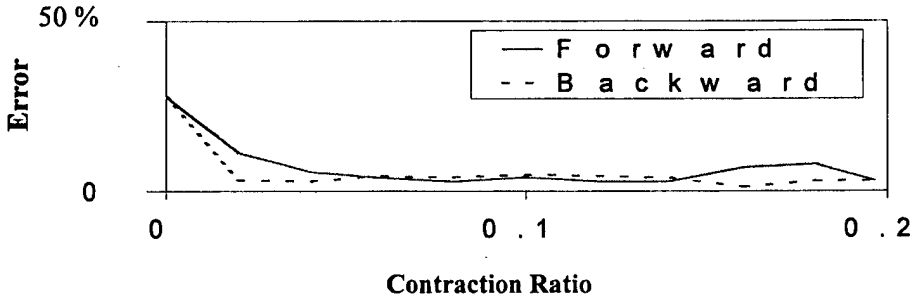

(b) P=56.8[psi]

Figure 3.7: Error between Model and Experimental Data (RUB-125)

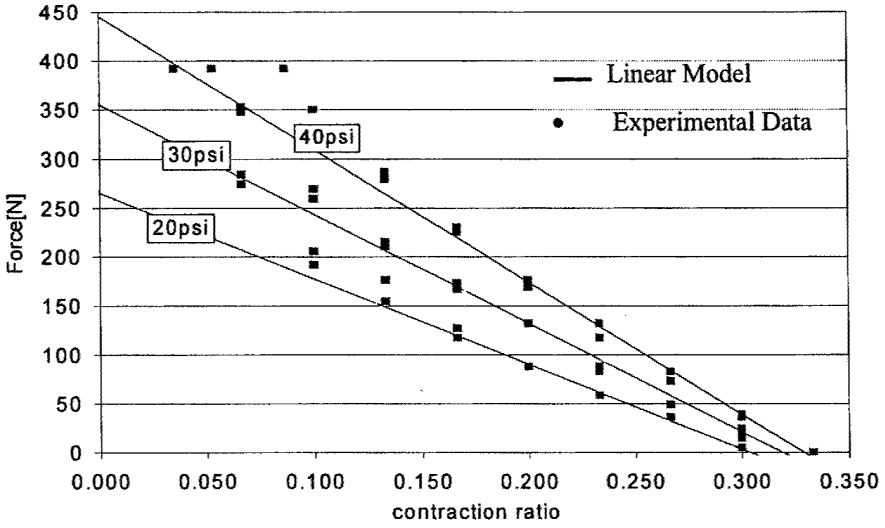

Figure 3.8: Experimental Modeling (AM-02)

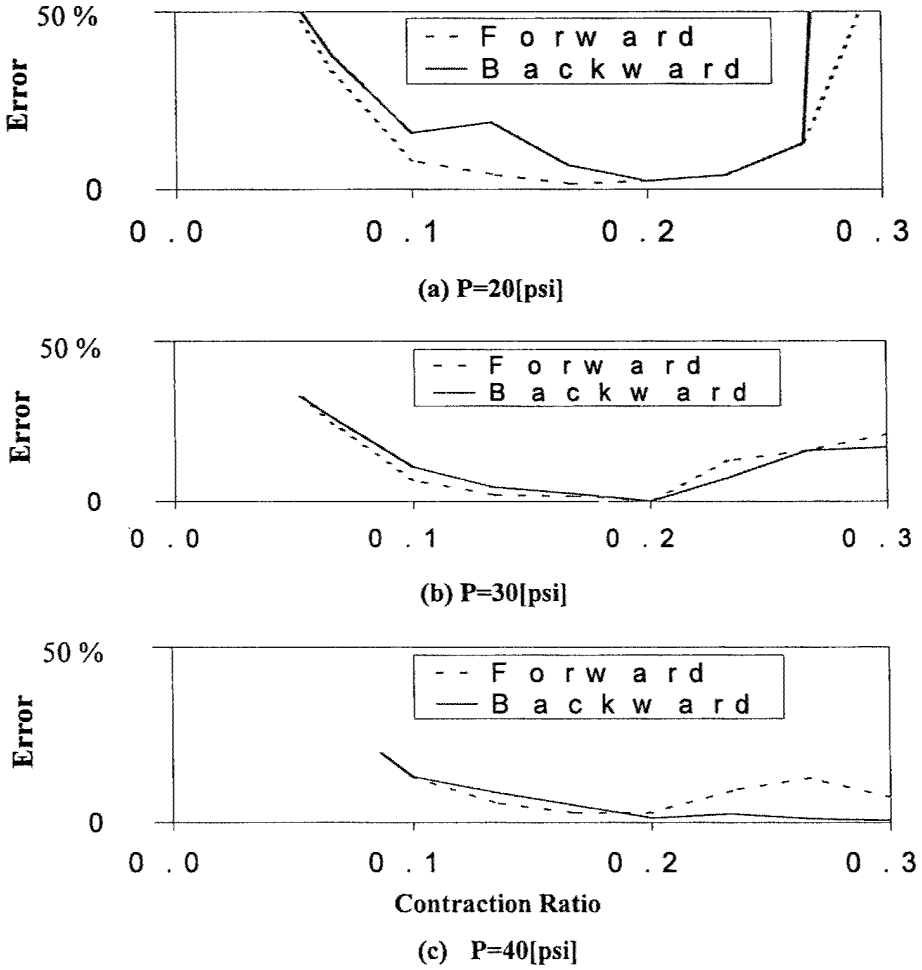

Figure 3.9: Error between Model and Experimental Data (AM-02)

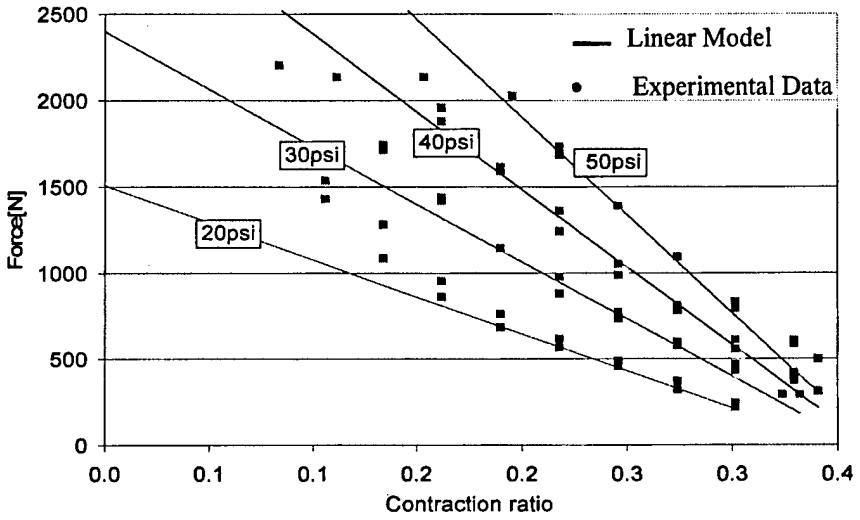

Figure 3.10: Experimental Modeling (AM-04)

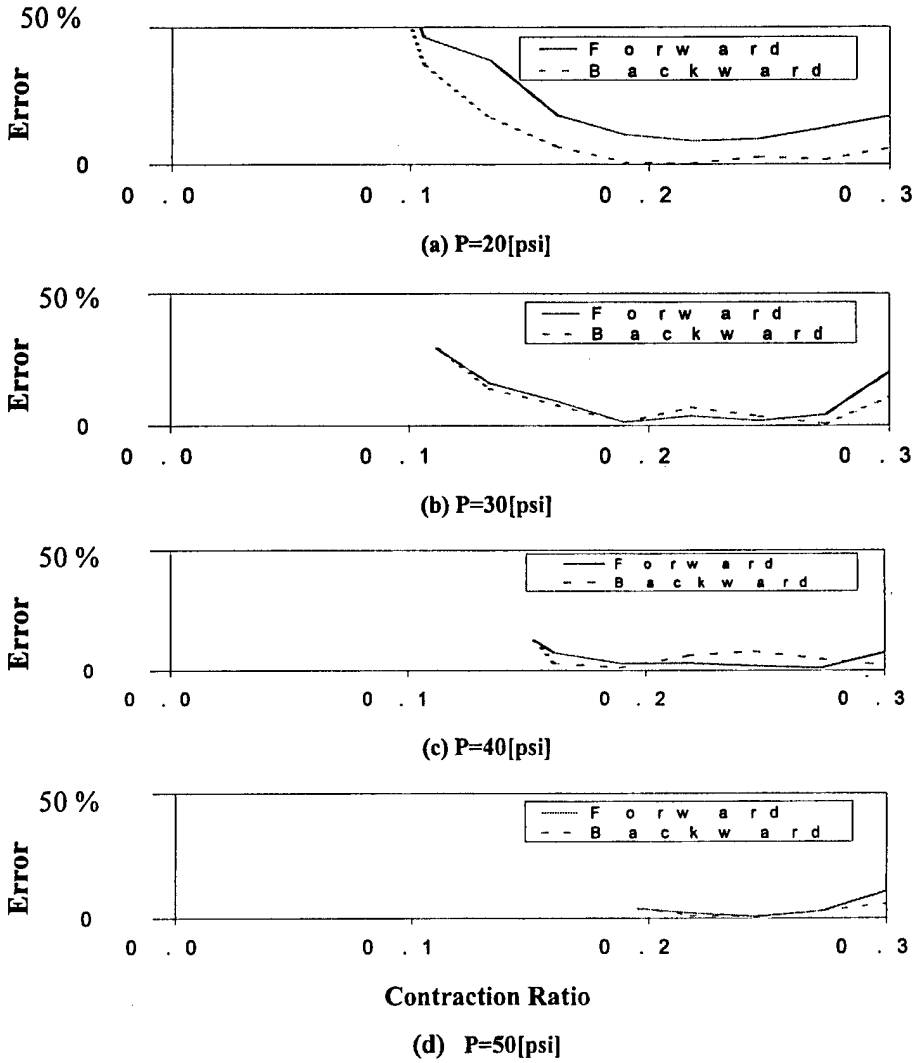

Figure 3.11: Error between Model and Experimental Data (AM-04)

3.3. Parameter Identification of Air Muscle

The identification of the parameters of air muscles, were done experimentally using the fixture shown in chapter 2. The simple depiction of the system is shown in Figure. 3.12.

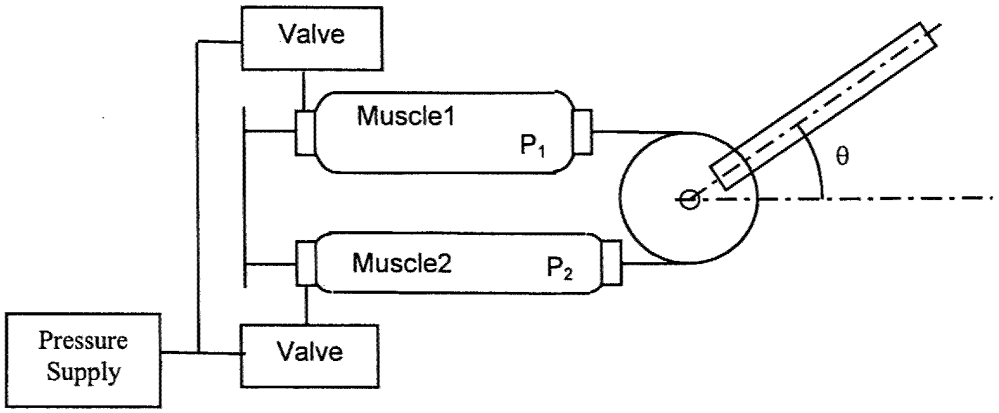

Figure 3.12: Construction of Air Muscle Actuator System

In this discussion the displacements were assumed to be small. As mentioned previously, the Equation of force vs. contraction for each ***i th*** muscle is given by

$$F_i = (aP_i + b)\varepsilon_i + (cP_i + d) \tag{3.30}$$

3.3.1. The Equation of Motion

With the assumption that P_i and δ_i change infinite decimal amounts from the basic pressure P_0 and basic contraction ratio ε_0 (ε under $P = P_0$),

$$P_i = P_{0i} + \delta P_i \tag{3.31}$$

$$\varepsilon_i = \varepsilon_{0i} + \delta\varepsilon_i \tag{3.32}$$

$$\delta\varepsilon_1 = -\delta\varepsilon_2 = \frac{r\theta}{L_n} \tag{3.33}$$

where,

R = The radius of the pulley

θ = The angle of rotation

L_n = The natural length of the air muscle

Substituting these Equations into Equation 3.30 yields,

$$F_i = (aP_{0i}\varepsilon_{0i} + b\varepsilon_{0i} + cP_{0i} + d) + (a\varepsilon_{0i} + c)\delta P_i + (aP_{0i} + b)\delta\varepsilon_i + a\delta P_i\delta\varepsilon_i \tag{3.34}$$

If it is assumed that

$$F_i = F_{0i} + \delta F_i \tag{3.35}$$

then,

$$\delta F_i = Ka \cdot \delta P_i + Kb \cdot \delta\varepsilon_i \tag{3.36}$$

where,

$$F_{0i} = aP_{0i}\varepsilon_{0i} + b\varepsilon_{0i} + cP_{0i} + d$$

$$\begin{aligned} Ka &= a\varepsilon_{0i} + c \\ Kb &= aP_{0i} + b \end{aligned} \tag{3.37}$$

$$a\delta P_i\delta\varepsilon_i \approx 0$$

Using these Equations, the dynamic Equation of motion can be obtained as follows.

The moment M at the pulley with the link is

$$M = (F_1 - F_2) \cdot r \tag{3.38}$$

where, F_i and F_2 are the contraction force of muscle 1 and muscle 2 respectively.

If the force of each muscle under basic pressure is $F_{01} = F_{02}$,then

$$M = (\delta F_1 - \delta F_2) \cdot r \tag{3.39}$$

Substituting Equation 3.36 into Equation 3.39 yields

$$M = \{Ka(\delta P_1 - \delta P_2) + Kb(\delta \varepsilon_1 - \delta \varepsilon_2)\} \cdot r \tag{3.40}$$

Substituting Equation 3.33 into Equation 3.40 yields

$$M = Ka \cdot r(\delta P_1 - \delta P_2) + Kb \cdot r \cdot \left(\frac{2r\theta}{L_n}\right) \tag{3.41}$$

thus

$$M = Ka \cdot r(\delta P_1 - \delta P_2) + \frac{2Kb\, r^2}{L_n}\theta \tag{3.42}$$

Finally, the moment M of the rotating parts can be described as

$$M = Kc(\delta P_1 - \delta P_2) - Kd \cdot \theta \tag{3.43}$$

where,

$$Kc = Ka \cdot r$$
$$Kd = -\frac{2Kb \cdot r^2}{L_n} \tag{3.44}$$

The Equation of motion is shown as

$$J\ddot{\theta} + c\dot{\theta} = M \tag{3.45}$$

where,

J= The moment of inertia of the wheel and the link

C= Damping coefficient

Substituting Equation 3.43 into Equation 3.45 yields

$$J\ddot{\theta} + c\dot{\theta} + Kd\theta = Kc(\delta P_1 - \delta P_2) \tag{3.46}$$

3.3.2. *Parameter Identification by Experiment*

The parameters K_d and c in Equation 3.46 can be obtained by using the free vibration of our system. The system was subjected to an initial angle while keeping the pressure of both muscles at basic pressure P_0. The back and forward motion of the link was recorded. The results of each muscle are shown in Figure.3.13.

If both muscles are kept at the same constant pressure, the Equation 3.46 can be expressed as

$$J\ddot{\theta} + c\dot{\theta} + Kd\theta = 0 \tag{3.47}$$

Dividing the Equation by J yields

$$\ddot{\theta} + 2\zeta\omega_n\dot{\theta} + \omega_n^2\theta = 0 \tag{3.48}$$

where,

ζ: Damping ratio

ω_n: Natural frequency

and

$$Kd = J\omega_n^2 \tag{3.49}$$

$$c = 2J\zeta\omega_n \tag{3.50}$$

Also

$$\omega_n = \frac{2\pi}{T} \tag{3.51}$$

Substituting these into Equation 3.49 and Equation 3.50 respectively, yields

$$Kd = \frac{4\pi^2 J}{T^2} \tag{3.52}$$

$$c = \frac{4\pi\zeta J}{T^2} \tag{3.53}$$

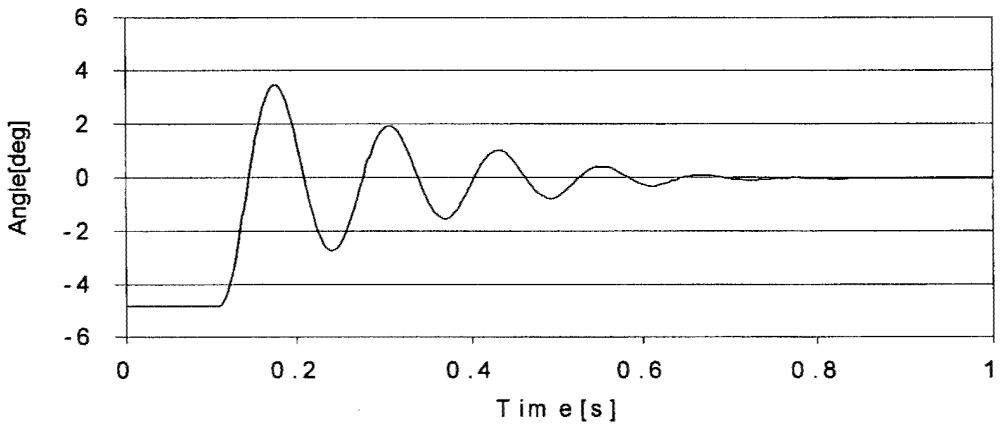

RUB-125 muscle

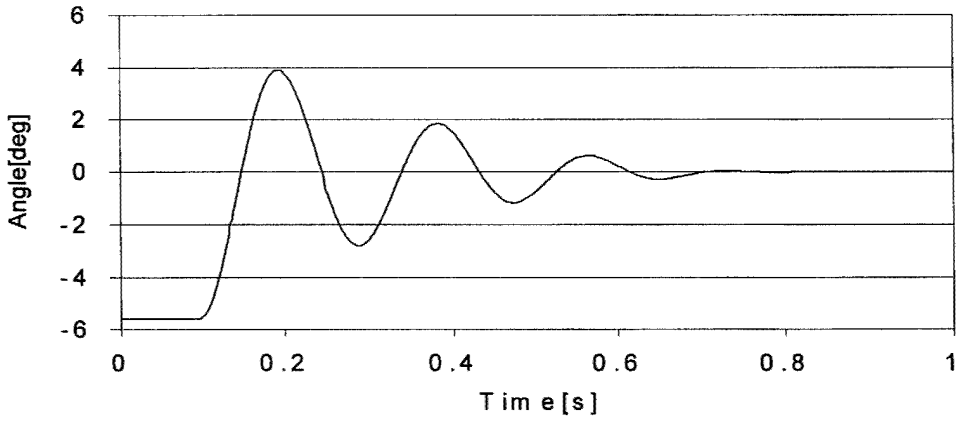

AM-02 muscle

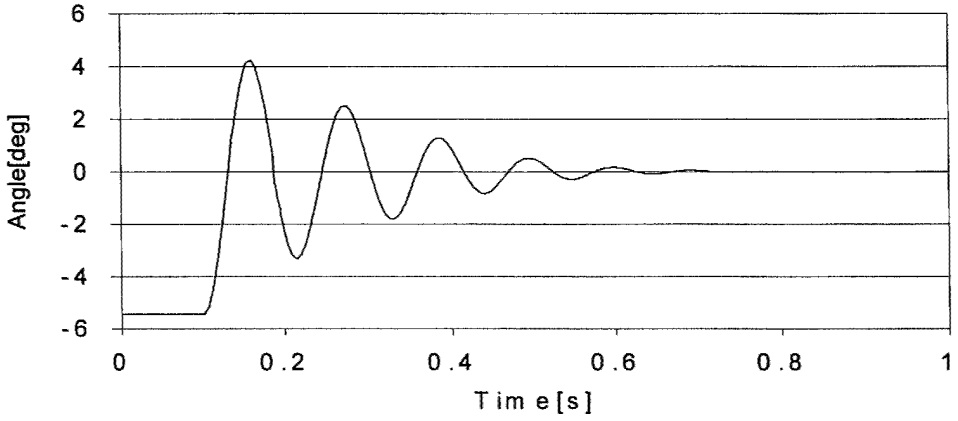

AM-04 muscle

Figure 3.13: Free Vibration of Link

The period T and the damping ratio ζ. are obtained using the recorded data of free vibration. Then substituting these parameters into Equation 3.52 and Equation 3.53 the parameters Kd and c are obtained.

The parameter Kc was determined by performing the static tests to obtain the relationship between the difference of pressure change (δP_1 -δP_2) of each muscle and the angle of θ.

If the moment M = 0 then the Equation 3.43 can be simplified as

$$Kc = \frac{Kd}{\delta P_1 - \delta P_2}\theta \tag{3.54}$$

if $P_{01} = P_{02}$ in Equation 3.31 then

$$\Delta P = \delta P_1 - \delta P_2 = P_1 - P_2 \tag{3.55}$$

Therefore, Equation 3.54 becomes

$$Kc = \frac{\theta}{\Delta P} \cdot Kd \tag{3.56}$$

The experimental results obtained from the relationship between θ and ΔP, are shown in Figure. 3.14. The values of parameters obtained from three types of muscles using experimental results are shown in Table 3.2.

Table 3.2: Parameter Values Identified by Free Vibration Experiment

	Kd[Nm/rad]	c [Nm/(rad/s)]	$\theta/\Delta P$[rad/Pa]
RUB-125	**82.2**	**0.476**	**$-2.0\ 10^{-6}$**
AM-02	**12.7**	**0.243**	**$-6.76\ 10^{-7}$**
AM-04	**114.5**	**0.605**	**$-1.77\ 10^{-6}$**

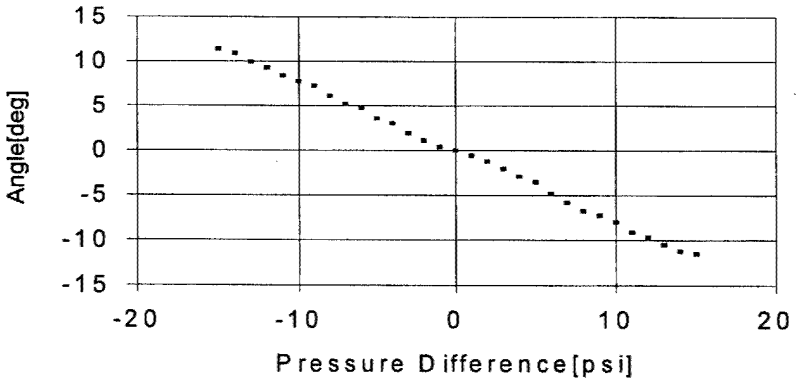

RUB-125

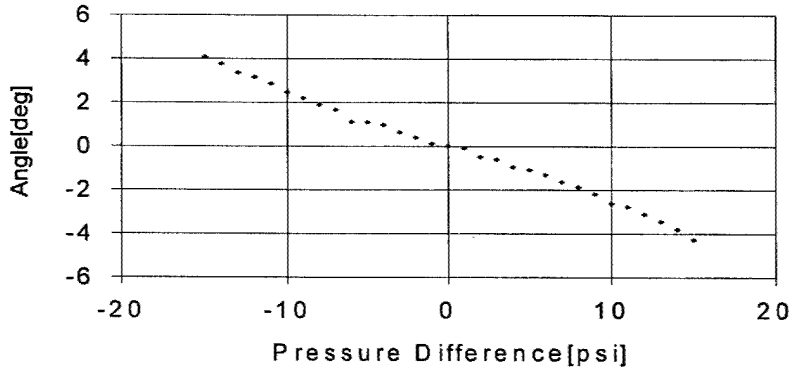

AM-02

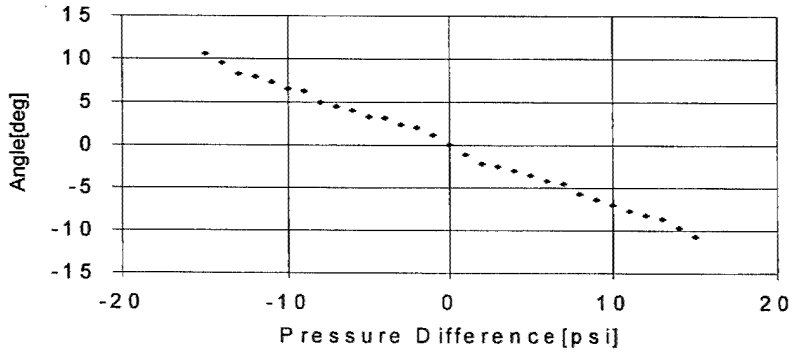

(c) AM-04

Figure 3.14: Relationship between Angle and Pressure Difference

4. System Control and Response

With the analytical model established and its parameters experimentally identified, algorithms were developed for controlling the angular displacement of the link though position control of a pair of pneumatic muscles. First, Proportional Integral (PI) control was applied which resulted in a time delay of desired response. Then a Feed-Forward control algorithm was developed and applied, which successfully compensated the time delay in muscle response.

4.1. PI Control

The encoder measured the angular displacement of the pulley and this signal was sent to the computer. The computer then sent a pressure control signal to the proportional pressure control valves of the two muscles based on the difference of the measured angle and a reference angle. The control signal is based on the PI control shown as follows.

$$\delta P_r = K_P \theta_e + K_I \int \theta_e dt \tag{4.1}$$

$$\begin{aligned} P_{r1} &= P_{01} + \delta P_r / 2 \\ P_{r2} &= P_{02} - \delta P_r / 2 \end{aligned} \tag{4.2}$$

where,

$\theta_e = \theta_r - \theta$: difference between the reference angle and the measured angle

P_{r1}, P_{r2}: pressure control signals for muscle 1 and muscle 2

K_P : proportional gain

K_I : integral gain

The output voltage signals sent to the pressure control valves are

$$V_i = K_V P_{ri}$$

where,

K_V (i=1, 2): coefficient of the valve based on the relationship between input voltage and output pressure

Step responses under the PI control were obtained through experiments and compared with the results simulated using the experimental model shown in Equation 3.29. Figure 4.1 show the experimental and simulated results for each type of the muscles, where the reference signal was set at 5 degrees. The parameter values used in the experiments and simulation are shown in Table 4.1.

In the case of RUB-125 and AM-02 muscles, the experimental and simulated responses agreed well, except for their frequencies. Ignoring the friction of threads and the elasticity of bladder when modeling the muscle actuator system, mainly caused the difference in frequencies.

In case of the largest size muscle, AM-04, the experimental result did not well correlate with the simulated one. Due to the large air capacity of the muscle and the small inlet to supply air, the response velocity of muscle was limited, which was, not considered in the analytical model. From the experimental data, it can be confirmed that the maximum contraction velocity under the basic pressure around 35[psi] is 8.64[mm/s]. Therefore, for a step control signal, the required response velocity exceeded the maximum velocity capacity of the muscle and, as a result, the muscle contracts at its maximum velocity.

In summary, the simulated response reasonably agreed well with the experimental response, indicating that the analytical model together with its parameters identified in this study is sufficient.

Table 4.1: Parameter Values for PI Control

PARAMETERS	RUB-125	AM-02	AM-04
J [kgm^2]	**0.029**		
r [m]	**0.045**		
L_n [m]	**0.225**	**0.160**	**0.358**
C [Nm/(rad/s)]	**0.476**	**0.243**	**0.605**
T [s]	**0.118**	**0.3**	**0.1**
ζ	**0.154**	**0.2**	**0.166**
K_c [m^3]	$\mathbf{1.644 \times 10^{-4}}$	$\mathbf{8.599 \times 10^{-6}}$	$\mathbf{2.029 \times 10^{-4}}$
K_d [Nm/rad]	**82.22**	**12.72**	**114.49**
K_p[[psi/rad]	**65**	**120**	**100**
K_i[[psi/rad.sec]	**1000**	**1300**	**800**

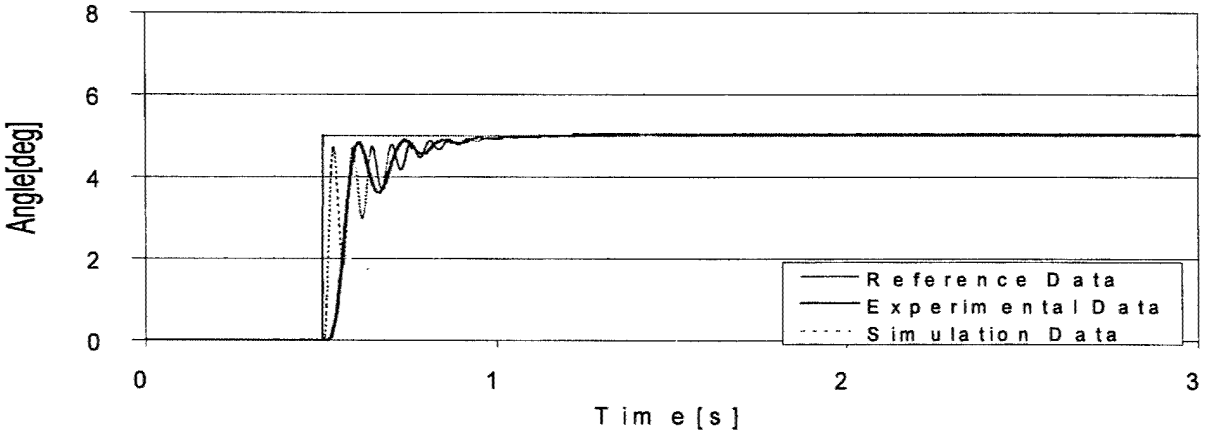

(a) RUB-125

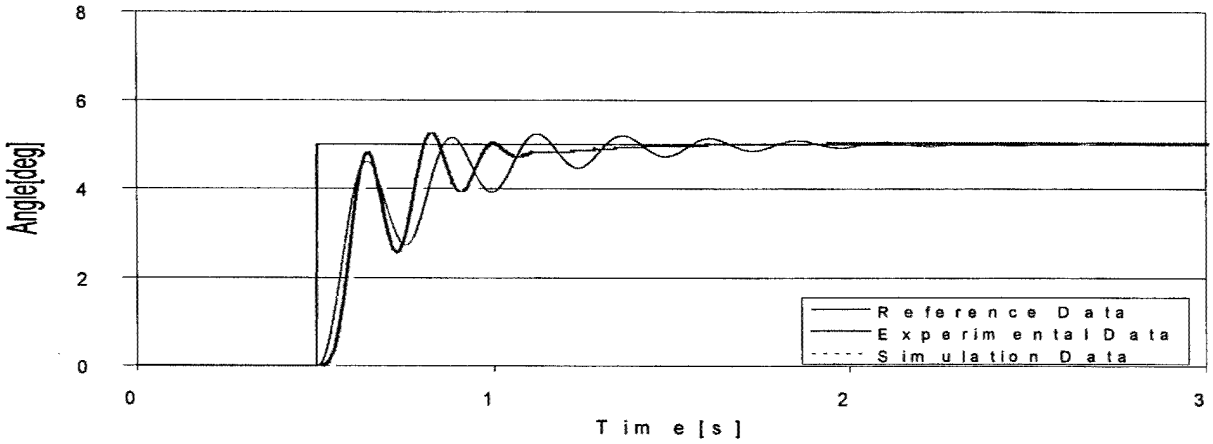

(b) AM-02

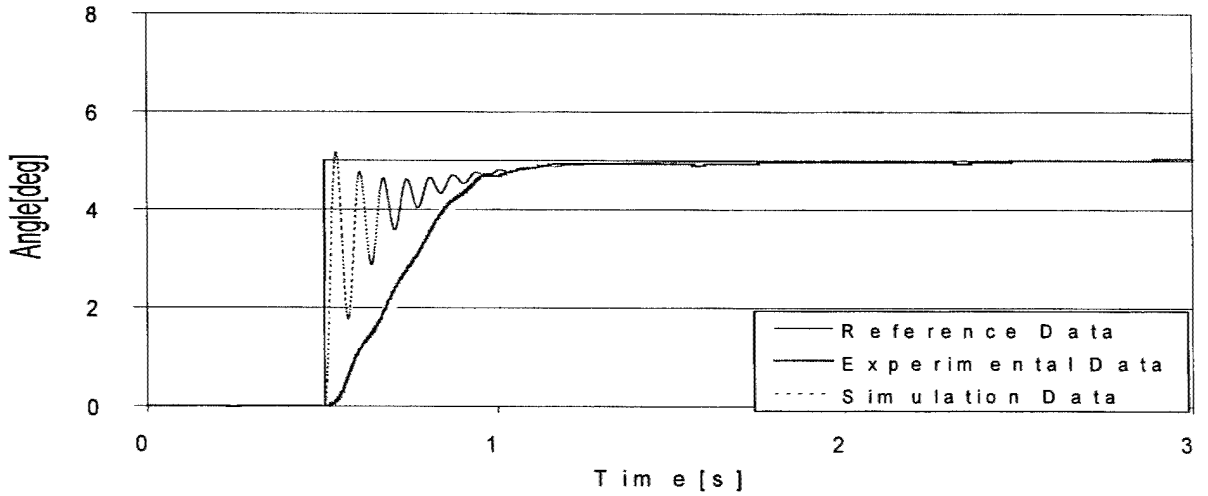

(c) AM-04

Figure 4.1: Step Response of PI Control

4.2. Compensation using Feed-Forward Control

This section documents the results of feed-forward control that was used to control the movement of the link arm in a predetermined path. The path sought was a sine curve. Time delay of air muscle system was shown in Figure 4.1. A feed-forward control algorithm was thus developed to compensate the time delay.

The control system equipped with the feed-forward algorithm is shown in Figure. 4.2 (Noritsugu et al, 1986). The gain K_{fp} was decided by the static relationship between the angular displacement and the difference of pressures ΔP, which was discussed in Chapter 3.3.2. In addition, a low pass filter was added with a time constant T = 0.125 seconds to alleviate the rapid change in velocity of motion. Adding a differential motion with gain of K_{fv} also helped to compensate the delay.

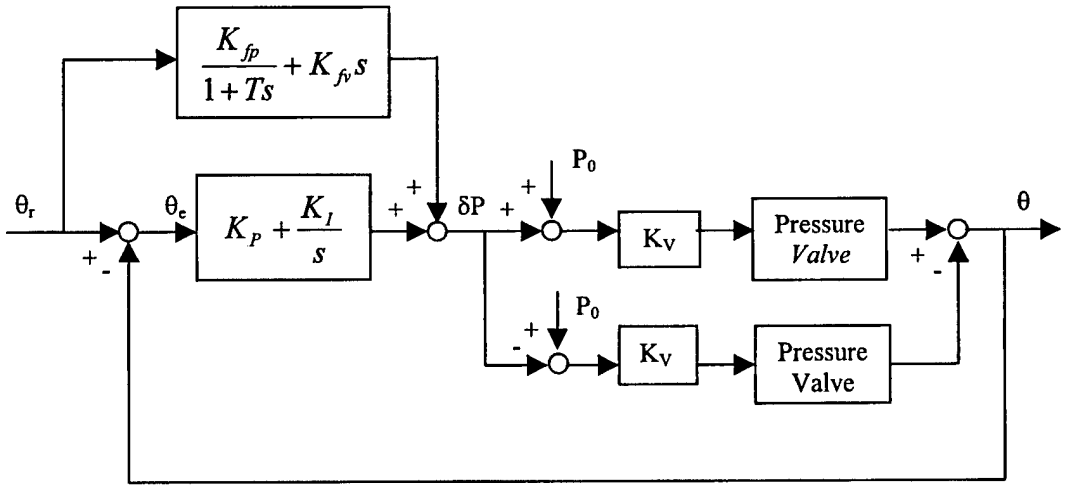

Figure 4.2: Control with Feed-Forward Compensation

The angular displacement of the link arm was controlled to follow a sinusoidal curve with an amplitude of 5 degrees and a period of 2 seconds for muscles RUB-125 and AM-02, and 4 seconds for muscle AM-04. The Figure 4.3 shows the response of each type of muscle system under the PI control without feed-forward compensation. In this case when compared with the reference signal, time delay in response is again demonstrated.

The sinusoidal response under the feed-forward control is shown in Figure.4.4. The parameter values of the control system are shown in Table 4.2. Considering the limited velocity capacity of muscle AM-04, sinusoidal signals with higher frequencies (period less than 4 seconds) were not tested. Compared with the results under the PI control without feed-forward compensation shown in Figure. 4.3, the results under the feed-forward control were significantly better in terms of the reduction of time delay. The maximum error between the reference and measured signals is reduced to about 0.3 degrees. The instability demonstrated at the early stages of the time history is due to the discontinuity of the velocity at the starting point.

Table 4.2: Parameter Values for Control with Feed-Forward Compensation

	RUB-125	AM-02	AM-04
$K_{fp\ [psi/rad]}$	100	245	102
$K_{fv\ [psi*s/rad]}$	20	45	45
$K_{p\ [psi/rad]}$	100	120	1500
$K_{i\ [psi/(rad*s)]}$	20	280	3800

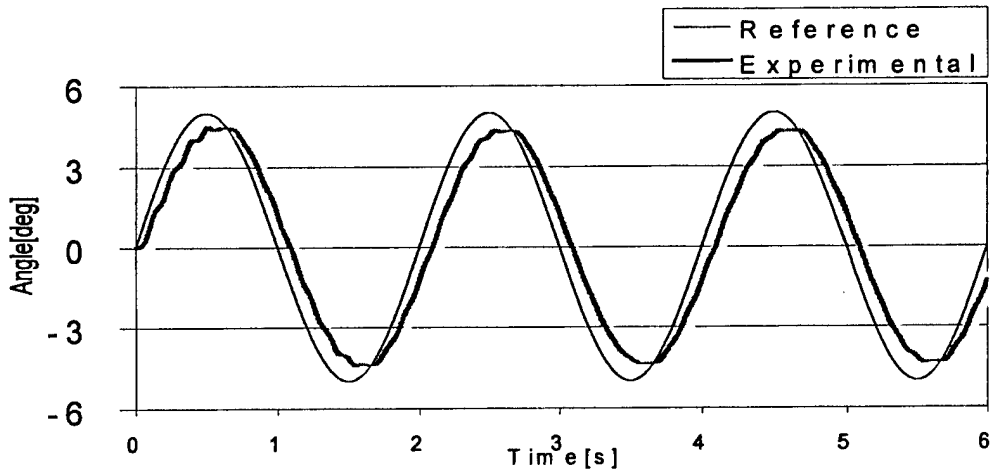

RUB-125

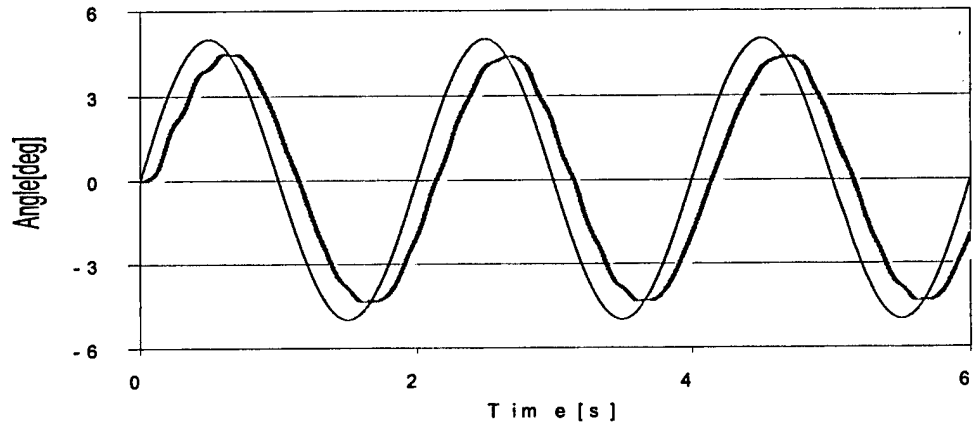

AM-02

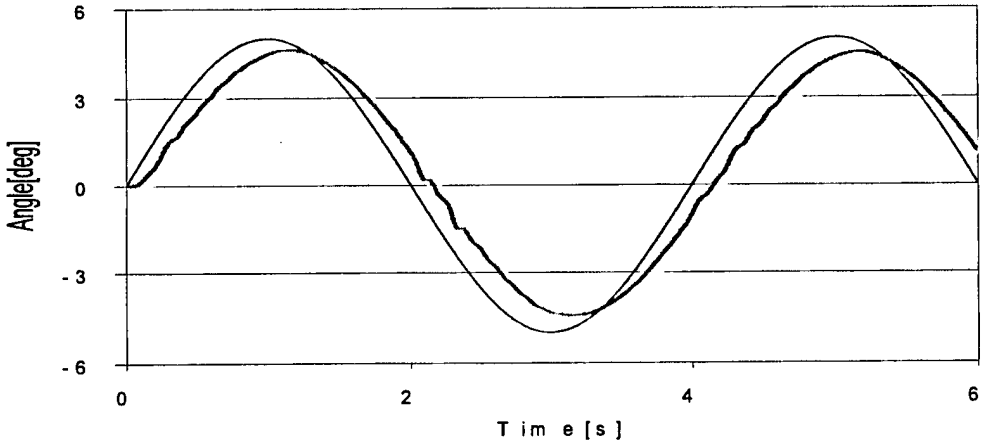

AM-04

Figure 4.3: Experimental Results of PI Control

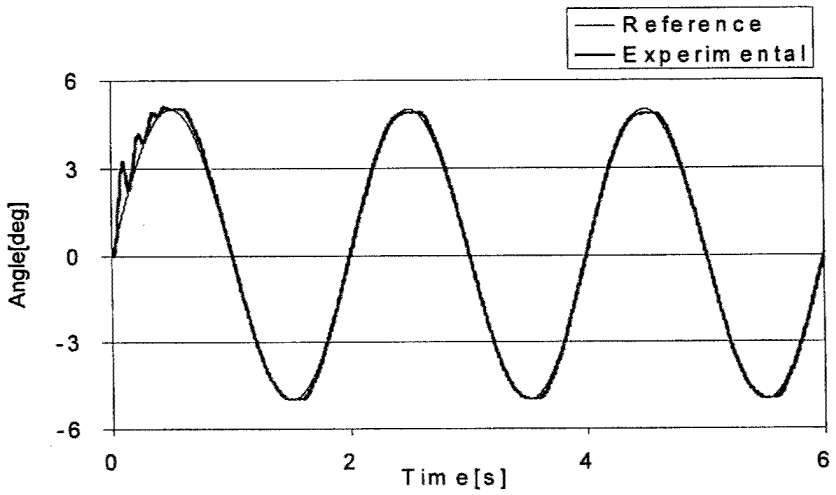

RUB-125

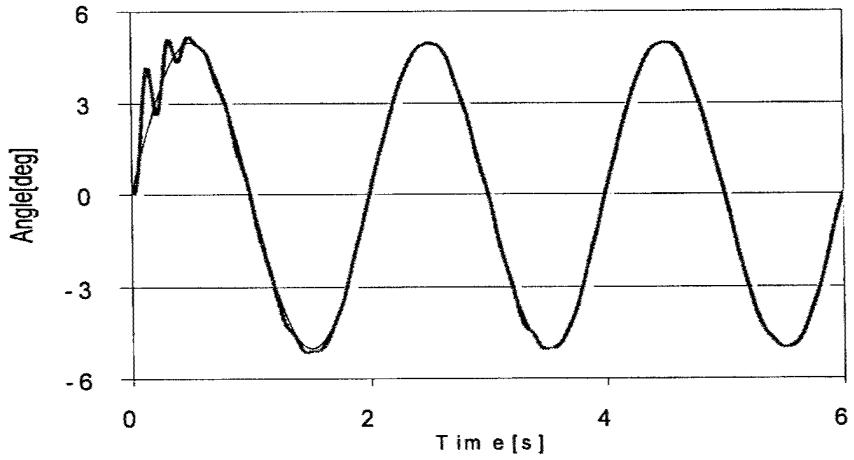

AM-02

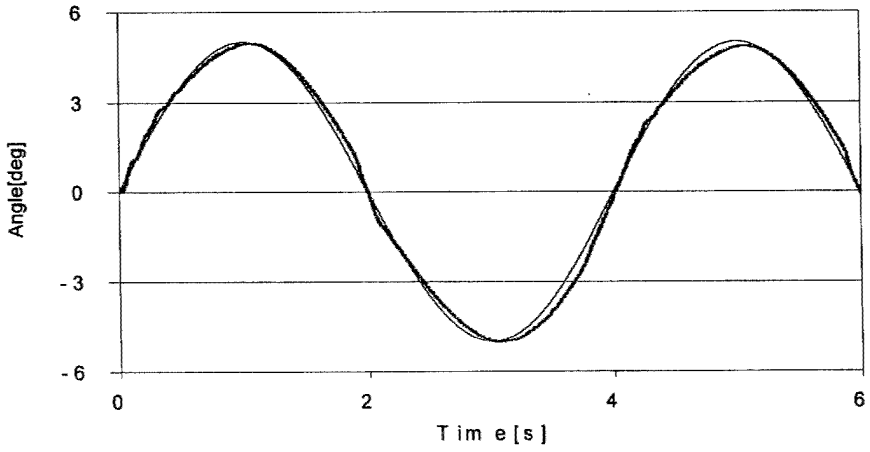

AM-04

Figure 4.4: Control with Feed-Forward Compensation

5. Summary and Conclusions

The following tasks have been performed in this research project:

1. A prototype pneumatic rubber muscle actuator system has been designed and fabricated which consists a pair of muscles and a pulley, resembling a human arm joint. An encoder was installed to measure the rotation of the pulley driven by the muscles and two pressure sensors to measure the pressure inside the rubber blades. Air was supplied from an air compressor through two servo values. This system was connected to a computer through I/O boards including A/D and D/A converters.
2. Three types of rubber muscles with different manufacturers and different sizes have been tested.
3. The theoretical model of the muscle system (relationship among the pressure, contraction ratio and force) was found quite different from the experimental data. As a result, experiments were performed to develop a model and to identify its parameter values, rather than using the theoretical model. The developed model was used for designing the control system.
4. Control algorithms were developed including a feed-forward algorithm to compensate the time delay of the muscle system.

The following observations and conclusions can be made from this research:

1. The linearity of the muscle actuator depends on the manufacturing quality. Based on the criterion determined in this study, the linear range of the Bridgestone muscles was found to be as large as 97 [%] of its stroke, while the that of the two Shadow muscles only reached 22 [%] and 23 [%] of their strokes respectively.

2. The accuracy of the analytical model of the muscle system experimentally developed in this study was demonstrated through comparison of the experimental and analytical step responses.

3. The time delay of the muscle response depends on the size of the muscle. The larger muscle suffers from longer time delay, although it provides larger power and stroke.

4. The control algorithm equipped with a feed-forward compensation developed in this research is very effective in reducing the time delay in response.

5. Excellent control performance of the pneumatic muscle actuator system was demonstrated by experiments.

6. Bibliography

C. P. Chou and B. Hannaford, "Measurement and modeling of McKibben pneumatic artificial muscles", *IEEE Transactions on Robotics and Automation*, Vol. 12, No. 1, 1996, pp. 90-102.

M. Q. Feng, T. Kobayashi, and K. Yamafuji, "An attitude-controllable free-falling robot cat", *To be submitted to IEEE Transactions on Robotics and Automation*, 1997.

M. M. Gavrilovic and M. R. Maric, "Positional servo-mechanism activated by artificial muscles", *Med. & Biol. Eng.*, Vol. 7, 1969, pp. 77-82.

D. G. Galdwell, G. A. Medrano-Cerda, and M. Goodwin: "Control of pneumatic muscle actuators", *IEEE Control Systems*, Vol. 15, No. 1, 1995, pp. 40-48

T. Hesselroth, K. Sarkar, P. v. d. Smagt, and k. Schulten, "Neural network control and a pneumatic robot arm", *IEEE Transactions on Systems. Man. and Cybernetics*, Vol. 24, No. 1, 1994, pp. 28-38

K. Inoue, "Rubbertuators and applications for robots", *Robotics Research: The 4th Int'l Symp.*, R. Bolles, and B. Roth Eds. Cambridge, MA: MIT Press, 1988.

D. W. Repperger, C. A. Phippips, R. D. Harmon, and K.R. Johnson, " A study of Pneumatic muscle Technology for Possible Assistance in Mobility," 1997

H. F. Schulte, Jr., "The characteristics of the McKibben artificial muscle", *The application of External Power in Prosthetics and Orthotics*, Washington, DC: Nat. Acad. Sci - Nat. Res. Council, 1961.

M. Uno, "Rubber artificial muscles and their applications in robotics", *Hydraulic and Pneumatic Actuation*, Vol, 17, No. 3, 1986, pp. 175-179. (in Japanese)

K. Yamafuji, K. Honda, and T. Kobayashi, "Midair posture detection and landing control of a robot with multiarticulated twin legs", *Transactions of JSME (C)*, Vol. 59, No. 565, 1993, pp. 188-195, (in Japanese)

T. Noritsugu, F. Ando, and T. Yoshikawa, "Control Performance of Rubber Artificial Muscle", Proc. of the 35th Symposium of Automatic Control Association, 1991. (in Japanese)

Appendix

I). Written publications in technical journals

R. Purasinghe, M Feng, S. Moromugi, M. Shinozuka, A. Bhaumik, X. Wei, E. Mercado, W.Olmedo, " Development of High Performance Actuator Systems," **in preparation to be submitted** to Transactions on Mechatronics, IEEE and ASME.

II). A list of professional personnel associated with the research effort

(California State University at Los Angeles)

i) Rupa Pursinghe, Principle Investigator

ii) Anjan Bhaumik, Faculty Research Associate

iii) Xiang Wei, Graduate Student. MS Degree Graduate Directed Study Project

" Development of a High Performance Pneumatic-Muscle Actuator System"

M.S. Degree (expected), Winter 2000

iv) Edgar Mercado, Undergraduate Student

v) William Olmedo, Undergraduate/Graduate Student

Subcontractors:

i) Feng Enterprises

ii) University of Southern California

III). Papers presented at meetings, conferences, seminars, etc.

"Development of a Pneumatic Muscle Actuator System" Presented at the Civil and Environmental Engineering Conference - New Frontiers and Challenges, Asian Institute of Technology, Bangkok, Thailand, November 1999.